Mon. Not. R. Astron. Soc. **345,** 854–864 (2003)

Flaring up: radio diagnostics of the kinematic, hydrodynamic and environmental properties of gamma-ray bursts

Alicia M. Soderberg★† and Enrico Ramirez-Ruiz
Institute of Astronomy, Madingley Road, Cambridge, CB3 0HA

Accepted 2003 July 8. Received 2003 June 13; in original form 2002 October 24

ABSTRACT

The specific incidence of radio flares appears to be significantly larger than that of the prompt optical emission. This abundance, coupled with the reverse shock interpretation, suggests that radio flares add a unique probe on the physics of gamma-ray burst (GRB) shocks. Motivated thus, we estimate the strength of the reverse shock expected for bursts in which multiwavelength observations have allowed the physical parameters of the forward shock to be determined. We use all six bursts (980519, 990123, 990510, 991208, 991216, 000418) which are found to be adiabatic and thus are predicted to have a strong reverse shock. We aim to constrain the hydrodynamic evolution of the reverse shock and the initial bulk Lorentz factor – which we found to be between 10^2 and 10^3 and well above the lower limits derived from the requirement that GRBs be optically thin to high-energy photons. In half of the cases we improve the description of the early afterglow light curves by adding a contribution from the reverse shock. Modelling of this early emission provides the opportunity to investigate the immediate surroundings of the burst. For 991216 and 991208, the expected $1/r^2$ density structure for a stellar wind is not compatible with the early afterglow light curves. Considering the radial range relevant to these GRBs, we discuss the conditions under which the inclusion of a wind termination shock may resolve the absence of a $1/r^2$ density profile.

Key words: shock waves – supernovae: general – gamma-rays: bursts – X-rays: general.

1 INTRODUCTION

The prompt and extremely bright optical flash in the gamma-ray burst (GRB) 990123 (Akerlof et al. 1999) was accompanied by a strong radio flare (Kulkarni et al. 1999). Peaking at ∼1 d, the flare was unlike usual radio afterglows which rise to maximum on a timescale of weeks or even months. The simplest interpretation of this radio flare is that it arises from the reverse shock (RS) component of the external shock (Sari & Piran 1999, hereafter SP99). The RS propagates into the adiabatically cooled particles of the coasting ejecta, thereby shocking the shell material and producing a prompt optical flash. The RS emission then weakens rapidly and shifts to lower energies, eventually crossing the observed radio band. Indeed, it has been shown that the radio counterpart to GRB 990123 is compatible with estimates derived from scaling down the prompt optical emission to the epoch of the radio afterglow observations (Kulkarni et al. 1999).

It turns out that there is a broad range of model parameters for which a strong optical flash is expected to precede the main GRB afterglow (Soderberg & Ramirez-Ruiz 2002, hereafter SR02). Such flashes are, however, difficult to detect in the current observing modes (Akerlof et al. 2000; Paczyński 2001). On the other hand, the specific incidence of radio flares of 1:4 (Djorgovski et al. 2001) appears to be significantly larger than that of the prompt optical emission obtained by the Robotic Optical Transient Search Experiment (ROTSE; Kehoe et al. 2001) or the Livermore Optical Transient Imaging System (LOTIS; Williams et al. 2000). This abundance, together with the RS interpretation, suggests that the radio flare phenomenon has the potential to shed new light on the physics of GRBs. Motivated by this interpretation, we have estimated the strength of the radio flare expected from bursts in which broad-band observations have been able to constrain the physical parameters of the forward shock (FS) emission (Panaitescu & Kumar 2001b, 2002, hereafter PK02). We use all six bursts (980519, 990123, 990510, 991208, 991216, 000418) which are found to be adiabatic (i.e. $\nu_m < \nu_c$) for reasonable assumptions about Γ_0 and thus are predicted to have a strong RS. Radiative bursts (e.g. 970508) are not selected because the RS component is significantly quenched in this regime, and therefore the observations in these cases are dominated entirely by emission from the FS. By evolving prompt optical flux estimates to the epoch of radio afterglow observations, we are able to discern whether a contribution from the RS could have been detected. We find that for half of the bursts for which the cooling frequency

★E-mail: ams@astro.caltech.edu
†Present address: Department of Astronomy, 105-24, California Institute of Technology, Pasadena, CA 91125, USA.

is larger than the typical synchrotron frequency, the predicted RS emission (which is generally found to lie in the mildly relativistic temperature regime) combined with that of the FS produces an improved fit to the radio afterglow data. As we shall discuss, the strong dependence of the peak time of this radio flare on the bulk Lorentz factor Γ provides a way to measure this elusive parameter. Accepting the conclusion that the radio flare arises from the RS, we then place constraints on the velocity of source expansion and hence on the density and profile of the medium in the immediate vicinity of six bursts (980519, 990123, 990510, 991208, 991216, 000418). These constraints provide environmental diagnostics for GRBs and are compared with the main types of environments considered for afterglows. We assume $H_0 = 65$ km s^{-1} Mpc^{-1}, $\Omega_{\rm M} = 0.3$ and $\Omega_\Lambda = 0.7$.

2 THE REVERSE SHOCK: OPTICAL FLASH TO RADIO FLARE

Observations of the optical flash associated with GRB 990123 have confirmed earlier predictions of prompt emission from a RS (Mészáros & Rees 1999, hereafter MR99; SP99). Although it contains a comparable amount of internal energy to that of the FS, the RS bears a temperature which is significantly lower (typically by a factor of Γ). As it crosses the shell, the RS produces a single short burst of emission which is predicted to peak in the optical band with reasonable assumptions for the burst physical parameters (MR99). The time of peak emission, $t_{\rm peak}$, strongly depends on the initial bulk Lorentz factor of the burst. For high Γ_0 the peak time is comparable to the duration of the burst while for low Γ_0 it typically occurs at later times. More specifically, the peak time is defined as

$$t_{\rm peak} = \max[\Delta/c, t_{\rm dec}], \tag{1}$$

where Δ is the width of the shell. Here, $t_{\rm dec}$ is the time at which the inertia of the swept-up matter significantly decelerates the shell ejecta

$$t_{\rm dec} = \left(\frac{3E}{32\pi\Gamma_0^8 n_0 m_{\rm p} c^5}\right)^{1/3}, \tag{2}$$

where E is the isotropic energy of the burst and n_0 characterizes the density of the external medium (SP99). Δ can be inferred directly from the observed burst duration ($t_{\rm dur}$) by noting that $\Delta = ct_{\rm dur}/(1+z)$ and assuming the shell does not undergo significant spreading (Piran 1999). At a given time (e.g. $r_{\rm peak}$), the broad-band RS spectrum can be described by the ordering of the three synchrotron break frequencies: the self-absorption frequency $\nu_{\rm a}$, the cooling frequency $\nu_{\rm c}$ and the characteristic synchrotron frequency $\nu_{\rm m}$. For spectra with $\nu_{\rm a} < \nu_{\rm m} < \nu_{\rm c}$ the RS is adiabatic, while for $\nu_{\rm a} < \nu_{\rm c} < \nu_{\rm m}$ the RS is radiative, and so the electrons are cooled quickly. Although a radiative RS could demonstrate a peak flux of comparable brightness to an adiabatic blast wave, the emission would be rapidly quenched making it exceedingly difficult to detect.

2.1 Relativistic versus subrelativistic

The RS spectral break frequencies are easily calculated by comparing them to those of the FS (MR99; SP99; Panaitescu & Kumar 2000). By assuming equality of velocity and pressure across the contact discontinuity separating the shocks, it is possible to define the properties of the reverse-shocked region in terms of n_0 and Γ_0 (Blandford & McKee 1976, hereafter BM). However, unlike the FS, the RS is not always relativistic (Sari & Piran 1995). Shells satisfying

$$\xi \approx \left(\frac{E}{n_0 m_{\rm p} c^2}\right)^{1/6} \times \Delta^{-1/2}\Gamma_0^{-4/3} \gg 1 \tag{3}$$

are thin and are likely to have a Newtonian RS, which is typically too weak to decelerate the shell effectively. On the contrary, for thick shells ($\xi \ll 1$), the RS is relativistic and thus successfully described by the solution of BM. For an adiabatic blast wave peaking at $\nu_{\rm m}$, the thin shell spectral energy equations are given by

$$\nu_{\rm m} = 5.8\times10^{9}\epsilon_{e,-1}^{2}\epsilon_{B,-2}^{1/2}n_0^{1/2}\Gamma_0^{2}(1+z)^{-1/4}\,{\rm Hz} \tag{4}$$

$$F_{\nu,\rm max} = 4.2\times10^{-5}D_{28}^{-2}\epsilon_{B,-2}^{1/2}E_{50}n_0^{1/2}\Gamma_0(1+z)^{3/8}\,{\rm Jy}. \tag{5}$$

For the thick shell case we have

$$\nu_{\rm m} = 1\times10^{8}\epsilon_{e,-1}^{2}\epsilon_{B,-2}^{1/2}n_0^{1/2}\Gamma_0^{2}(1+z)^{-1/2}\,{\rm Hz} \tag{6}$$

$$F_{\nu,\rm max} = 6.0D_{28}^{-2}\epsilon_{B,-2}^{1/2}E_{50}^{5/4}n_0^{1/4}\Gamma_0^{-1}t_{\rm dur}^{-3/4}(1+z)^{1/2}\,{\rm Jy}, \tag{7}$$

where $F_{\nu,\rm max}$ is the spectral peak flux, $\epsilon_{\rm e}$ and ϵ_B are the equipartition functions for the electrons (e) and for the magnetic field (B) respectively, and D is the luminosity distance of the burst. Here we adopt the convention $Q = 10^x Q_x$ for expressing the physical parameters. It is important to note that in the thin shell regime $F_{\nu,\rm max}$ scales directly with Γ_0, while for the thick shell regime the relation is inverted.

2.2 Light curves of the reverse shock emission

Unlike the synchrotron spectrum, the afterglow light curve at a fixed frequency strongly depends on the hydrodynamics of the relativistic shell, which determines the temporal evolution of the break frequencies. In a mildly relativistic RS ($\xi > 1$), the temperature of the shocked material is non-relativistic and so the late-time evolution of the ejecta no longer follows the solution of BM. Furthermore, the Sedov–Taylor solution is not applicable due to the relativistic bulk Lorentz factor of the fluid (Kobayashi & Sari 2000, hereafter KS00). The hydrodynamic evolution of a mildly relativistic RS therefore lies in a regime for which there are no analytical solutions available. In order to constrain the evolution of Γ in this regime, it is common to assume (MR99; KS00)

$$\Gamma \propto R^{-g} \quad \text{with} \quad (3/2 \leqslant g \leqslant 7/2). \tag{8}$$

The limits on g reflect two evolutionary pathways of the pressure. Adiabatic expansion ($p \propto \rho^{4/3}$) is assumed for $g = 3/2$ while $g = 7/2$ corresponds to the case of pressure equilibrium, i.e. when the pressure of the FS matches that of the ejecta. Using the relation $t \propto R/\Gamma^2\, c$, we can obtain the scaling of Γ in terms of the observer–frame time, which is given by

$$\Gamma \propto t^{-g/(1+2g)}. \tag{9}$$

The pressure and density then scale as

$$p \propto t^{-8(3+g)/7(1+2g)} \qquad \rho \propto t^{-6(3+g)/7(1+2g)}. \tag{10}$$

The application of these scalings to a slow cooling RS gives the spectral evolution as a function of g. For an adiabatic blast wave, it can be shown that $\nu_{\rm m} \propto \Gamma p^{5/2}\rho^{-2}$ and $F_{\nu_{\rm m}} \propto \Gamma p^{1/2}$ (KS00). In terms of the observer–frame time, these scalings are then

$$\nu_{\rm m} \propto t^{-3(8+5g)/7(1+2g)} \qquad F_{\nu_m} \propto t^{-(12+11g)/7(1+2g)}. \tag{11}$$

Following the peak optical emission, with the passage of time, the light from the RS shifts rapidly to lower frequencies. After the RS peak frequency $\nu_{\rm m}$ crosses the observing frequency it decays rapidly. The evolution of the radio flux for frequencies above $\nu_{\rm m}$ is typically found by assuming a distribution of injected electrons with power

law of index p above a minimum Lorentz factor γ_i. The corresponding spectral flux at a given frequency above ν_m is then given by $F_\nu \approx F_{\nu_m}(\nu/\nu_m)^{-(p-1)/2}$; with $F_\nu \propto \nu^2$ at low frequencies ($\nu < \nu_a$) and $F_\nu \propto \nu^{1/3}$ bridging the two regimes. Together with the scalings of equation (11), the above expression gives the evolution of the radio flare immediately after the ν_m crossing:

$$F_\nu \propto T^{-(7+24p+15pg)/14(1+2g)}\nu > \nu_m. \quad (12)$$

It should be noted that, for a typical spectral index $p = 2.5$, the flux decay index varies in a relatively narrow range (≈0.4) between the theoretical limits of $g = [1/2, 3/2]$. Because the flux decay index is a monotonic function of g, it is not very sensitive to it, and consequently the decay shape is more strongly affected by the value of Γ_0 than of g. As demonstrated in Section 3, the quality of GRB radio observations is not yet sufficient to place robust constraints on g, and thus the hydrodynamic evolution of the RS is currently not well determined.

3 CONSTRAINING THE KINEMATICS AND HYDRODYNAMICAL EVOLUTION OF THE REVERSE SHOCK

Despite ongoing observational searches, GRB 990123 remains one of the few bursts for which a radio flare has been observed. The ability to detect flares depends on both the strength and peak time of the optical flash as well as the subsequent flux decay index. In turn, these observables depend on the ambiguous dynamics of the RS. By constraining the kinematic and hydrodynamic properties of the shock, we may enable observational strategies for radio flare detection to be improved. Moreover, as we will demonstrate, constraints on the physics of the RS may provide us with environmental diagnostics of GRBs. In this section, we present a method to determine the properties of the RS through modelling of the early radio afterglow observations. We constrain both the velocity of source expansion Γ_0 and the evolutionary index g of the RS in bursts for which multiwavelength observations have been able to determine the physical parameters of the FS. We use all six bursts (980519, 990123, 990510, 991208, 991216, 000418) which are found to be adiabatic (i.e. $\nu_m < \nu_c$) for reasonable assumptions about Γ_0. Assuming that the burst equipartition values for the FS are shared by the RS, we apply the formalism developed in the previous section to determine the spectral and temporal evolution of the RS. We estimate the strength of the RS contribution in the radio band during the epoch of afterglow observations. Through combining our radio flare estimates with predictions for the FS emission (obtained by PK02), we are able to estimate the combination of Γ_0 and g which provides the best χ^2 fit to the early radio data. We consider both cases where the temperature of the shocked shell is relativistic or not. This is particularly important because for reasonable assumptions about the velocity of source expansion we find in all cases that $\xi \sim 1$. For $\chi^2_{FS+RS}/\chi^2_{FS} < 1$, the fit is improved by including emission from the RS. We will show that, although current RS theory predicts a detectable radio flare component for a wide range of Γ_0 and g parameter values, it appears to be observationally supported for only some bursts. Below, we discuss the radio emission and RS modelling of the individual GRBs. A summary of results is listed in Table 1.

3.1 GRB 980519

The broad-band modelling of the FS emission by PK02 was found to overestimate the radio observations at early times. The addition of a RS contribution to the FS emission serves only to worsen the fit. Assuming the thin regime solution, we find that a minimum flux contribution is expected from the RS for $\Gamma_0 \sim 490$ and $g \sim 1.5$. Thick shell solutions for this burst do not converge because the predicted radio flare decreases indefinitely with increasing Γ_0. Therefore, we can only determine a lower limit of $\Gamma_0 > 230$ for this regime. These constraints imply a mildly relativistic RS with $\xi \sim 1$. In this case, neither the thick nor thin regimes are ruled out by the observations. For these values of Γ_0 and g, the radio observations are fit with a FS + RS emission model giving a similar χ^2 to that of the FS alone. We find a reduced $\chi^2 = 12$ and a ratio of the quality of the fits gives $\chi^2_{FS+RS}/\chi^2_{FS} = 1.4$ for the thin shell case (see Fig. 1). It should be noted that the χ^2 ratio can in principle decrease for values of $\Gamma_0 >$ 1000 and $g = 1.5$. However, with a peak time of only a few seconds, this solution is clearly inconsistent with the constraints given by equation (1). Therefore, by assuming the results for $\chi^2_{FS+RS}/\chi^2_{FS} =$ 1.4 as our best fit, we find this solution to be in agreement with the previous estimate by PK02 of $\Gamma_0 > 250$.

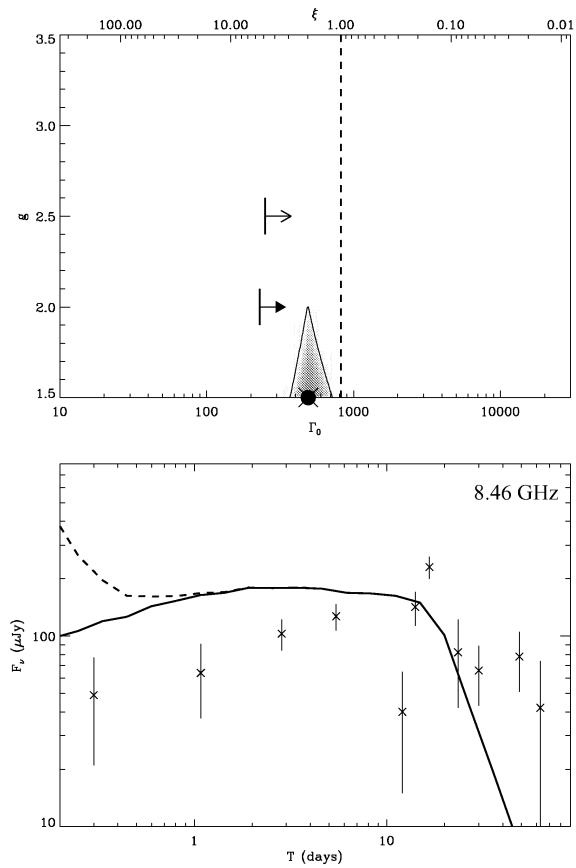

Figure 1. GRB 980519: constraints on Γ_0 and g assuming a thin shell. The best-fitting value is marked by a solid dot and the approximate 1σ uncertainty contour is shaded. The RS contribution can be minimized for values of $\Gamma_0 \sim 490$ and $g \sim 1.5$. Thick shell equations provide a lower limit of $\Gamma_0 > 230$ (filled arrow) which is consistent with $\Gamma_0 > 250$ derived by PK02. This RS is found to be mildly relativistic. Afterglow observations are fit better with a FS model (lower panel, solid line) than with a FS + RS model (lower panel, dashed line).

Here we comment on the structure of the χ^2 region for this burst as a representative of the larger sample included within this study. First, it should be noted that the unusual shape of the χ^2 region is the result of an intrinsic coupling between the fitted parameters, Γ_0 and g. Although a more proper treatment of the uncertainty region would include a full Monte Carlo analysis to determine the error

region, this level of complexity is not warranted by the quality of available data. We therefore apply standard χ^2 fitting techniques to build two-dimensional uncertainty regions and we emphasize that these represent only approximate confidence regions. Current theory dictates that the uncertainty region for Γ_0 has a lower boundary of $\Gamma_0 \sim 30$ due to the lack of photon–photon attenuation (Mészáros, Laguna & Rees 1993) and an upper boundary of $\Gamma_0 \sim 10^3$ based on the pulse width evolution of the prompt emission (Ramirez-Ruiz & Fenimore 2000). These theoretical bounds should be adopted as the overall uncertainty region for each of the bursts within this sample. Secondly, it should be noted that the sharp inflection points traced by the confidence region are an artefact of the discontinuity imposed by the transition from a non-relativistic to a relativistic regime. The tendency for the best-fitting value of g to favour the parameter space extrema demonstrates that Γ_0 is the dominant parameter in this model and thus the Lorentz factor drives the spectral evolution of the RS emission within this parameter space (as discussed in Section 2.2).

3.2 GRB 990123

Early radio observations of GRB 990123 revealed a flare rising to maximum after ∼1 d and then rapidly fading away (Kulkarni et al. 1999). The strong dimming of the radio emission after ∼2 d excluded a FS origin. The simplest interpretation was that it arises from the RS (Kulkarni et al. 1999; Panaitescu & Kumar 2000). As expected, the FS modelling by PK02 significantly underestimates the radio emission at the time of the flare. By including a RS contribution, a FS + RS emission model improves the fit by a factor of ∼100. Best-fitting values are obtained for $\Gamma_0 \sim 850$ ($\Gamma_0 \sim 240$) and $g \sim 3.4$ ($g \sim 3.3$) for the thin (thick) shell case (Figs 2 and 3). Both regimes predict a mildly relativistic RS with ξ values of ∼1 and ∼6 for the thin and thick shell solutions, respectively. Despite the differences between the regimes, both solutions show a minimum at $\chi^2_{\rm FS+RS} = 0.3$ which gives a ratio $\chi^2_{\rm FS+RS}/\chi^2_{\rm FS} \sim 0.01$, thus demonstrating a remarkable improvement to the FS fit. Note that the inclusion of self-absorption effects, which are not included in the FS model of PK01 or the FS + RS model presented here, may enable a better description of the radio observations before 1 d (the reader is referred to SP99 for this matter). It should be commented that, within the 1σ uncertainty region of the thin regime solution, there is a secondary minimum which occurs for lower Lorentz factors, near $\Gamma_0 \sim 400$ and $g \sim 3.5$. This solution corresponds to a peak time of 200 s, which is clearly inconsistent with the observed optical light curve that peaks at ∼50 s (Akerlof et al. 1999). Based on the observed behaviour of the optical flash, which is successfully described by a mildly relativistic shell (see Kobayashi 2000), we thus conclude that the thin shell solution is the regime which better describes the RS behaviour. We find the values of Γ_0 consistent with previous estimates for this burst: $\Gamma_0 \approx 1200$ (Wang, Dai & Lu 2000), $\Gamma_0 = 1400 \pm 700$ (Panaitescu & Kumar 2001a), $\Gamma_0 \approx 900 \pm 100$ (SR02), $\Gamma_0 > 180$ (Lithwick & Sari 2001, hereafter LS01), and $\Gamma_0 > 300$ (PK02). Estimates for the dimensionless thickness parameter, ξ, are similarly in agreement and include $\xi \sim 0.7$ (KS00) and $\xi = 0.99$ (SR02). Furthermore, the hydrodynamical evolution has previously been characterized by $g = 2.2$ (KS00) which is consistent within our approximate 1σ uncertainty region.

3.3 GRB 990510

As in the case of GRB 980519, the broad-band modelling of the FS emission of this burst overestimates the radio observations at early times (PK02). We find that a minimum flux contribution from the RS can be attained from the thin shell equations by setting $\Gamma_0 \sim 270$ and $g \sim 1.5$. The thick shell solution provides only a constraint of $\Gamma_0 > 230$. This RS is found to be mildly relativistic with $\xi \sim 1$. A FS + RS model gives a best-fitting value with $\chi^2 = 8.5$ and $\chi^2_{\rm FS+RS}/\chi^2_{\rm FS} \sim 8.0$ indicating that the standard FS fit is still preferred (see Fig. 4). A better χ^2 ratio (∼1) can be obtained for values of $\Gamma_0 > 2000$ and $g = 1.5$. We disregard this solution, however, as it corresponds to $t_{\rm peak} < 1$ s. Note that these results are in agreement with the estimate of $\Gamma_0 > 140$ derived by PK02 and the lower limit of $\Gamma_0 > 79$ by LS01.

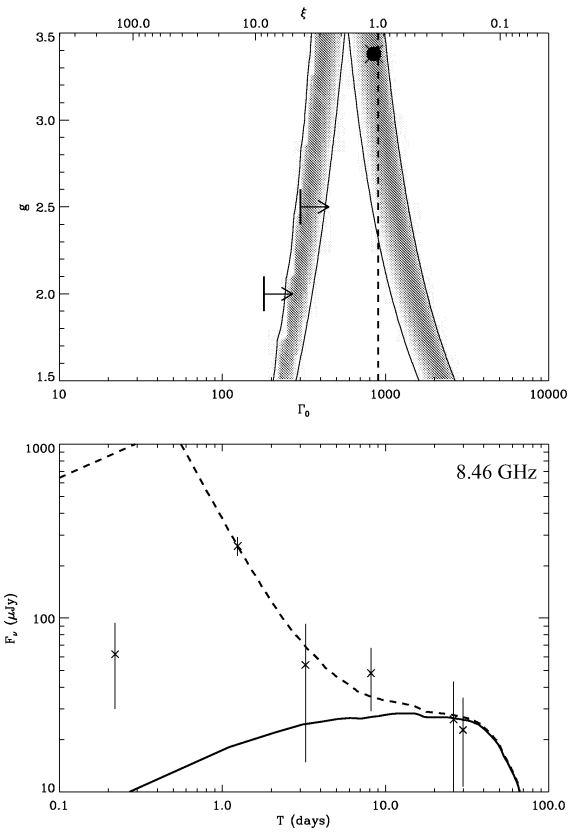

Figure 2. GRB 990123: Constraints on Γ_0 and g assuming a thin shell regime. Best-fitting values are marked by a solid dot and approximate 1σ uncertainty contours are shaded. Radio flare parameters, which produce the best fit to the data, are $\Gamma_0 \sim 850$ and $g \sim 3.4$ for the thin shell case. Best-fitting FS + RS light-curve models are plotted (dashed line) within the lower panel in order to compare with the FS model alone (solid line). The FS + RS model provides a significantly better fit to the radio emission. (Note the discrepancy associated with the first point is due to the effects of self-absorption.) The Γ_0 constraints are consistent with the estimate of $\Gamma_0 > 300$ (upper arrow) derived by PK02 and the lower limit of $\Gamma_0 > 180$ (lower arrow) by LS01. Note the mildly relativistic nature of the thin shell regimes, with $\xi \sim 1$.

3.4 GRB 991208

Broad-band fits to the FS of GRB 991208 included two sets of radio lights curves observed at 8.5 and 15 GHz. We calculate radio flare predictions for both observing frequencies. At 15 GHz, the FS prediction underestimates the data (PK02). By adding a RS contribution, we find the ratio $\chi^2_{\rm FS+RS}/\chi^2_{\rm FS}$ can be improved by a factor of ∼2 for both thin and thick solutions. Best FS + RS fits are

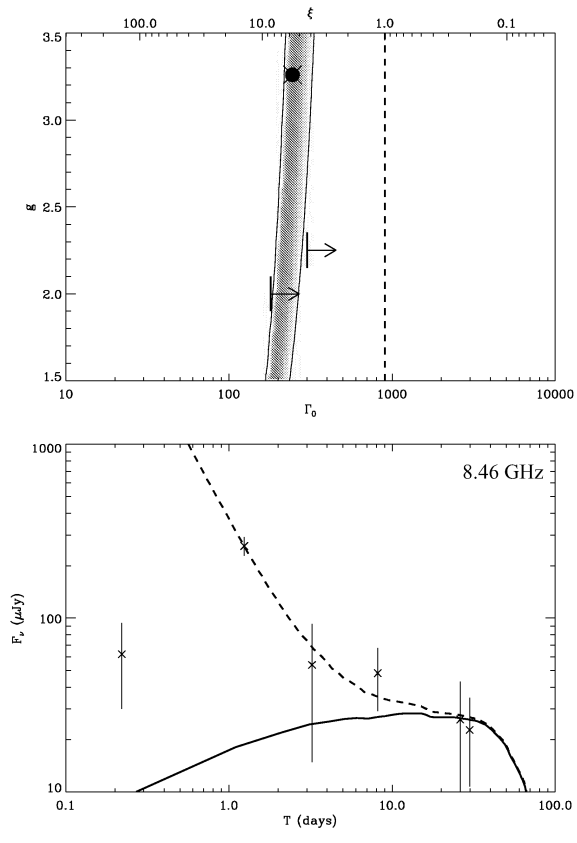

Figure 3. GRB 990123: Constraints on Γ_0 and g assuming a thick shell regime. Best-fitting values are marked by a solid dot and approximate 1σ uncertainty contours are shaded. Radio flare parameters, which produce the best fit to the data, are $\Gamma_0 \sim 240$ and $g \sim 3.3$ for the thick shell case. Best-fitting FS + RS light-curve models are plotted (dashed line) within the lower panel in order to compare with the FS model alone (solid line). It should be noted that the thin shell equations produce better fits to both radio and optical emission (see Fig. 2). The Γ_0 constraints are consistent with the estimate of $\Gamma_0 > 300$ (upper arrow) derived by PK02 and the lower limit of $\Gamma_0 > 180$ (lower arrow) by LS01. Note the mildly relativistic nature of the thick shell regimes, with $\xi \sim 6$.

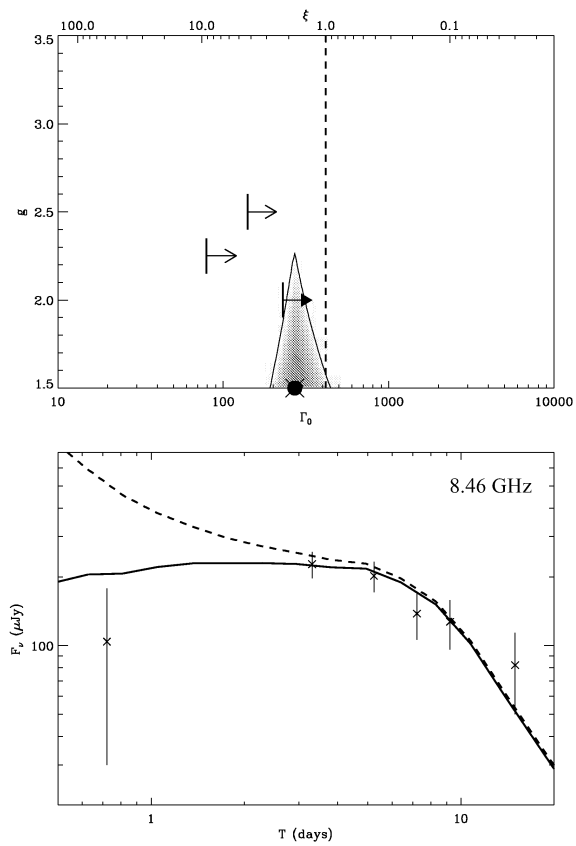

Figure 4. GRB 990510: Constraints on Γ_0 and g assuming a thin shell. The best-fitting value is marked by a solid dot and the approximate 1σ uncertainty contour is shaded. The radio flare is minimized for values of $\Gamma_0 \sim 270$ and $g \sim 1.5$ with $\xi \sim 2$. Thick shell equations provide a lower limit of $\Gamma_0 > 230$ (filled arrow) which is consistent with $\Gamma_0 > 140$ derived by PK02 (upper unfilled arrow) and $\Gamma_0 > 79$ by LS01 (lower unfilled arrow). Afterglow observations are better fit with a FS model (lower panel, solid line) than with a FS + RS model (lower panel, dashed line).

produced using $\Gamma_0 \sim 130$ and $g = 3.5$ for the thick shell equations, which give $\chi^2_{\rm FS+RS} \sim 1.5$ and a ratio of $\chi^2_{\rm FS+RS}/\chi^2_{\rm FS} \sim 0.4$. The thin shell solution is similar in quality, with best values of $\Gamma_0 \sim 110$ and $g \sim 1.9$, giving $\chi^2_{\rm FS+RS} \sim 1.9$ and a ratio of $\chi^2_{\rm FS+RS}/\chi^2_{\rm FS} \sim 0.5$. Both regimes predict a mildly relativistic RS with $\xi \sim 1$. At 8.5 GHz, a thin RS is unable to provide solutions which improve the FS fit. The best result gives $\chi^2_{\rm FS+RS}/\chi^2_{\rm FS} \sim 1.4$ for values of $\Gamma_0 \sim 110$ and $g \sim 1.5$. Thick shell equations fail to converge and therefore predict only a lower limit of $\Gamma_0 > 130$. Combining the two solution sets should generally enable further constraints. For this case, however, combining the sets merely reproduces the 15-GHz solution because this set of results is statistically dominant. Therefore, we quote the 15-GHz results as our best fits for this RS solution (Figs 5 and 6). Notice that the results are consistent with the PK02 limit of $\Gamma_0 > 68$.

3.5 GRB 991216

Early radio observations of GRB 991216 suggest the emission was already in decline after $t \sim 1$ d Frail et al. (2000). As a result, efforts to fit the radio light curve with a standard FS emission model proved difficult. Broad-band fits by Panaitescu & Kumar (2000) underestimate the early radio observations and claim that interstellar scintillation is essential in explaining the departures between observations and model fluxes. Alternative models have also been suggested, including a dual fireball, and a RS flare (Frail et al. 2000; Panaitescu & Kumar 2000). We find that the fit can be improved by a factor of ∼2 by including emission from the RS. Both thick and thin shell solutions give $\chi^2_{\rm FS+RS} \sim 4.2$. The thin shell solution favours a mildly relativistic RS with best-fitting values of $\Gamma_0 \sim 680$ and $g \sim 1.55$ (Fig. 7), while the thick shell solution gives a highly relativistic solution with $\Gamma_0 \sim 1200$ and $g \sim 1.5$ (Fig. 8). We note that this solution corresponds to a peak time less than ∼2 s which is considerably smaller than the estimated light width of the shell ∼15 s. Both thick and thin regimes produce RS solutions which are consistent with the PK02 constraint of $\Gamma_0 > 150$.

3.6 GRB 000418

Broad-band afterglow fits to the FS emission are in agreement with the radio observations (Berger et al. 2001; PK02). It is clear that the addition of a RS contribution will not improve the fit to the radio light curve. A minimum flux contribution is expected from the RS for $\Gamma_0 \sim 150$ and $g \sim 1.5$ assuming a thin shell (Fig. 9). This implies

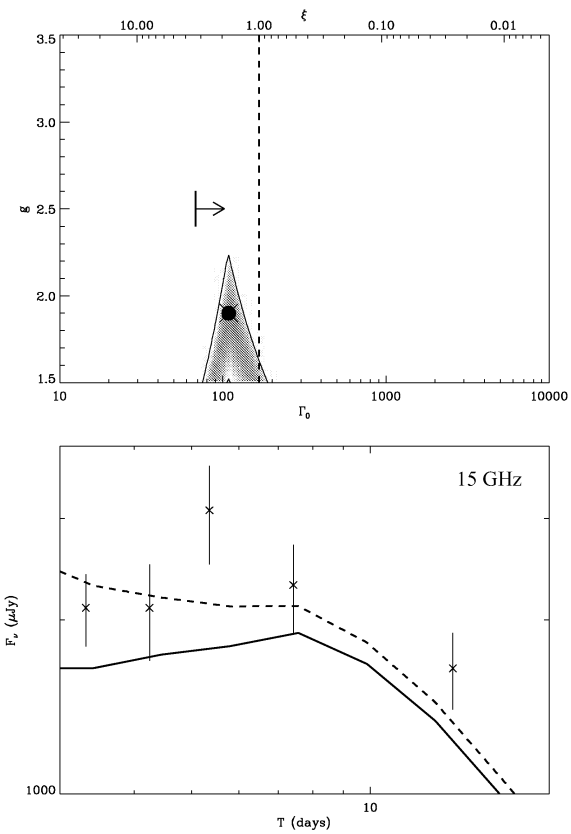

Figure 5. GRB 991208: Constraints on Γ_0 and g assuming a thin shell. The best-fitting value is marked by a solid dot and the approximate 1σ uncertainty contour is shaded. Best parameter fits are $\Gamma_0 \sim 110$ and $g \sim 1.9$ for $\chi^2 \sim 1.9$. Both the thick and thin shell regimes favour mildly relativistic solutions with $\xi \sim 1$. The FS + RS model (lower panel, dashed line) improves the quality of the light-curve fit by a factor of ∼2.5 as compared with the FS model (lower panel, solid line). Results are consistent with the PK02 constraint of $\Gamma_0 > 68$ (arrow).

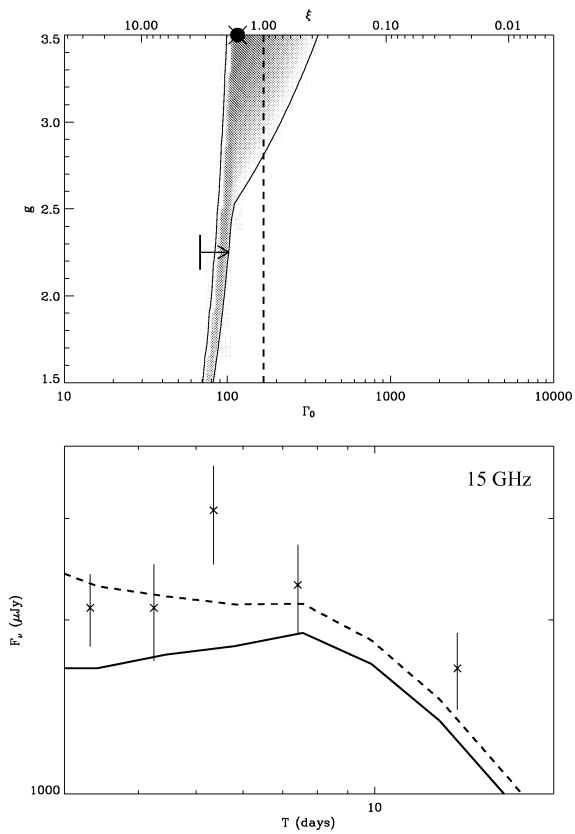

Figure 6. GRB 991208: Constraints on Γ_0 and g assuming a thick shell. The best-fitting value is marked by a solid dot and the approximate 1σ uncertainty contour is shaded. Best parameter fits are $\Gamma_0 \sim 130$ and $g \sim 3.5$ for $\chi^2 \sim 1.5$. Both the thick and thin shell regimes favour mildly relativistic solutions with $\xi \sim 1$. The FS + RS model (lower panel, dashed line) improves the quality of the light-curve fit by a factor of ∼2 as compared with the FS model (lower panel, solid line). Results are consistent with the PK02 constraint of $\Gamma_0 > 68$ (arrow).

a mildly relativistic RS with $\xi \sim 2$. The radio flux in the thick shell solution decreases with increasing bulk Lorentz factor and thus we can only determine a lower limit of $\Gamma_0 > 50$ for this regime. It is emphasized that the χ^2 ratio never falls below 1 (with the best-fitting $\chi^2_{\rm FS+RS} \sim 9.7$) for all values of Γ_0 and g. It should also be noted that the relatively large uncertainty region for this burst is due to the predicted faintness of the radio flare at the epoch of observations (∼10 d).

3.7 Caveats

A number of caveats apply to our analysis. First and foremost, the hydrodynamical and kinematical constraints presented here have been calculated under the assumption that the radio flare arises from the RS component of the blast wave (MR99; SP99). Within the grounds of the FS model, the radio flare (and, in particular, those observed in 990123, 991216 and 991208) can be accounted for only if the characteristic frequencies can be evolved much faster than that given by standard dynamics (as argued also by Kulkarni et al. 1999, for 990123). In contrast, the RS model provides a natural and consistent explanation for the radio flare.

In the framework of 'standard' afterglow models – by which we mean models that assume a power-law-shocked particle spectrum and a constant fraction of energy in electrons and magnetic fields relative to the thermal energy of the shocked particles – we have estimated the RS spectra by assuming that the equipartition values for the FS component are unchanged across the contact discontinuity. Although the validity of this assumption is questionable, it is a convenient method of estimating these illusive parameters until more is known about the microphysics of GRB shocks. We test the strength of this assumption by altering ϵ_B (the parameter for which there is larger uncertainty) by two to three orders of magnitude. The effect of strongly increasing ϵ_B is only a slight shift in the Γ_0–g confidence regions. Such shifts, however, are always found to lie within the uncertainty regions given for each burst, thus supporting the validity of our results.

The premise of our work has been that the physical parameters derived by PK02 provide a robust description of the FS emission. Most importantly, we assume that the PK02 parameters are not significantly biased by neglecting the effects of a RS component. This assumption is supported by the fact that the PK02 results are weighted towards the optical and X-ray data where the sampling frequency was large, the observational errors were small, and the RS component was negligible on time-scales ∼1 d. With sparse observations and large error bars, the radio data clearly do not constrain the multifrequency fit at the same level as the optical. The RS predictions presented here, for all bursts in our sample, proved to be generally consistent with the observed light curves, and it is critical to note that

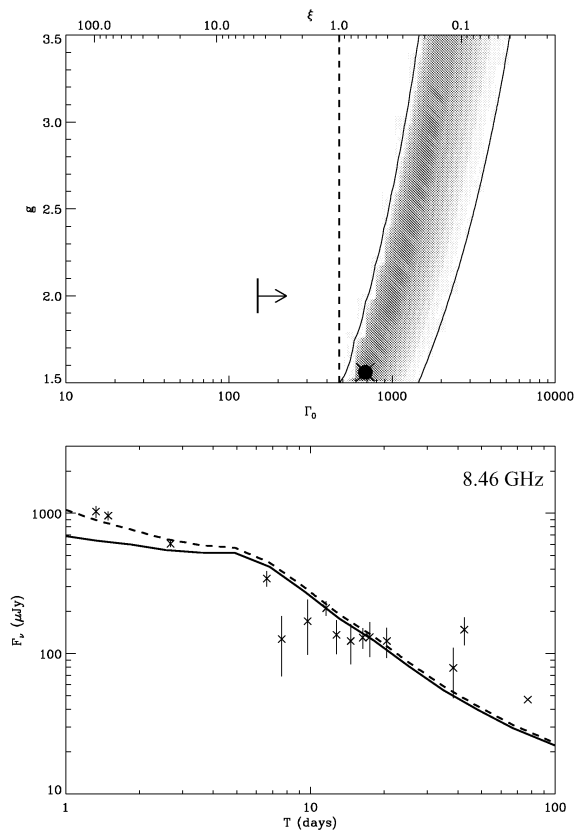

Figure 7. GRB 991216: Constraints on Γ_0 and g assuming a thin shell. The best-fitting value is marked by a solid dot and the approximate 1σ uncertainty contour is shaded. RS parameters which produce the best fit to the data are $\Gamma_0 \sim 680$ and $g \sim 1.55$ for $\chi^2 \sim 4.2$. The lower panel compares the best-fitting FS + RS light-curve model (dashed line) and the FS model alone (solid line). This value of Γ_0 is consistent with the PK02 constraint of $\Gamma_0 > 150$ (arrow). Note that the thin solution favours a mildly relativistic RS.

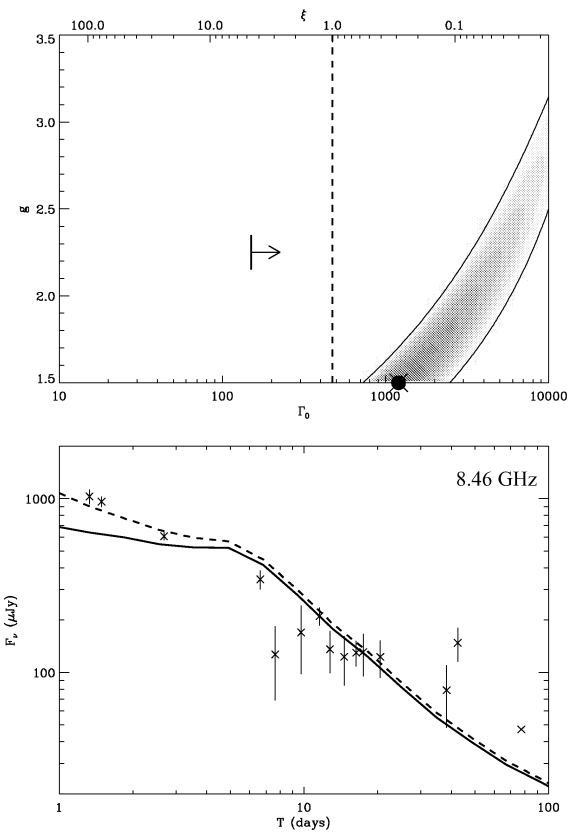

Figure 8. GRB 991216: Constraints on Γ_0 and g assuming a thick shell. The best-fitting value is marked by a solid dot and the approximate 1σ uncertainty contour is shaded. RS parameters which produce the best fit to the data are $\Gamma_0 \sim 1200$ and $g \sim 1.5$ for a thick shell. The lower panel compares the best-fitting FS + RS light-curve model (dashed line) and the FS model alone (solid line). This value of Γ_0 is consistent with the PK02 constraint of $\Gamma_0 > 150$ (arrow). In comparison with the thin shell constraint, the thick solution tends towards the relativistic limit with $\xi < 1$.

none of the RS predictions significantly overestimated the observed radio emission, even at early times. Our RS predictions therefore provide consistency checks for the physical parameters of PK02, which we find to be in agreement.

4 THE ELUSIVE Γ_0

As discussed in SR02, the bulk Lorentz factor plays a critical role in the majority of GRB emission models (see Piran 1999, for a review). The Lorentz factor, however, has also proven to be one of the most difficult physical parameters to constrain from GRB observations. Based on theoretical predictions and sparse observations, present estimates stretch over two orders of magnitude: $\Gamma_0 \approx 10$–10^3 (e.g. Mészáros et al. 1993; Wang et al. 2000; Ramirez-Ruiz & Fenimore 2000; PK02; LS01; SR02). Here we present constraints on Γ_0 for six of the best-sampled bursts observed to date. Although the Γ_0 constraints are still quite broad in some cases (e.g. 000418), information may still be gained from the collective Γ_0 distribution for our data set. As a method of investigating this, we treat each burst's constraint as a probability distribution and produce a total histogram by summing over the six normalized distributions. Specifically, for each burst, we construct a one-dimensional probability histogram for Γ_0, given by $p_i(\Gamma)\,\mathrm{d}\Gamma$. Here, $p_i(\Gamma)\,\mathrm{d}\Gamma$ represents the frequency of each $\mathrm{d}\Gamma$ value within the 1σ Γ_0–g confidence region. The $p_i(\Gamma)\,\mathrm{d}\Gamma$ probability histograms are each normalized to unity before summing them to create a total probability histogram, constructed as $p(\Gamma)\,\mathrm{d}\Gamma = \sum_i \mathrm{p_i}(\Gamma)\,\mathrm{d}\Gamma$. Fig. 10 plots the total probability histogram for the data set as a shaded and smoothed curve. A Gaussian fit to the total histogram is overplotted with a mean value of $\Gamma_0 = 150$. It should be noted that the distribution is weighted heavily to the Γ_0 constraints derived for GRB 991208, because this burst was the most tightly constrained within the data set (due to additional observations at 15 GHz). To remove this burst from the total probability histogram leaves five bursts with radio flare constraints derived from 8.46-GHz data only. The total probability histogram associated with this smaller set of bursts has a larger mean bulk Lorentz factor, which may represent the collective constraints more accurately, with $\Gamma_0 = 270$. We emphasize that this mean value is consistent with lower limits on Γ_0 as derived by LS01 for a set of 12 bursts and also with estimates for Γ_0 by PK02 for 10 bursts. As additional Γ_0 constraints are gathered from future bursts, the distribution of Lorentz factors should offer vital clues concerning the diversity of GRB source expansion velocities.

5 GRB ENVIRONMENTS AND PROGENITORS

Models for the GRB afterglows indicate that the emission comes from a region $\sim 10^{16}$–10^{18} cm from the source of the explosion.

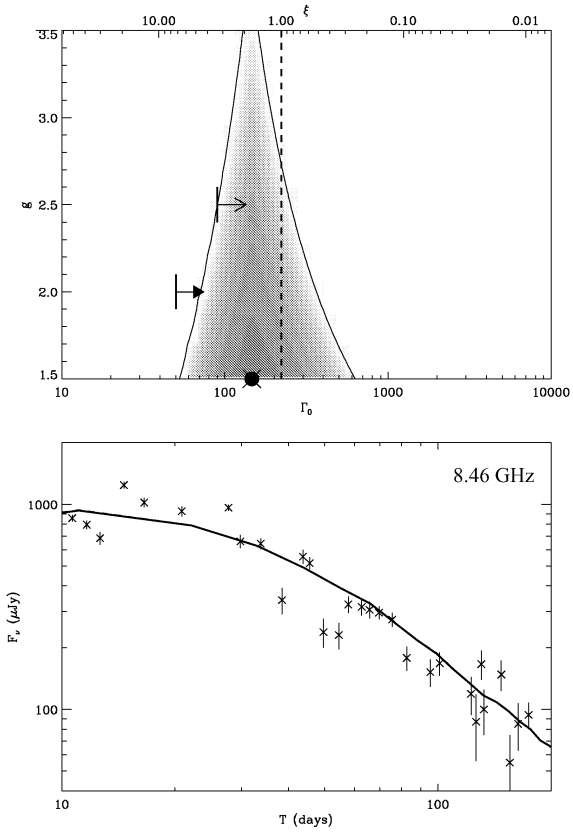

Figure 9. GRB 000418: Constraints on Γ_0 and g assuming a thin RS. The best-fitting value is marked by a solid dot and the approximate 1σ uncertainty contour is shaded. The RS contribution can be minimized for values of $\Gamma_0 \sim 150$ and $g \sim 1.5$. Thick shell equations provide a lower limit of $\Gamma_0 > 50$ (filled arrow) which is less constraining than $\Gamma_0 > 90$ as derived from jet modelling (PK02). This shock is mildly relativistic with $\xi \sim 1.7$. The lower panel compares the resulting best-fitting FS + RS light-curve model (dashed line) with the FS model (solid line).

The nature of the material depends on the GRB progenitors, which are at present not known. The question of a wind versus a constant density medium is a crucial one, because massive stars, one of the leading candidates for GRB progenitors (e.g. Woosley 1993; Paczyński 1998), should be surrounded by a $\rho \propto r^{-2}$ wind (unless a supernova explosion occurs before the burst; Vietri & Stella 1998; Konigl & Granot 2002; Guetta & Granot 2003). In contrast, GRBs resulting from compact star mergers, the other leading candidate, are expected to be surrounded by the interstellar medium (Lattimer & Schramm 1976; Paczyński 1986; Narayan Paczynéski & Piran 1992; Perna & Belczynski 2002; Rosswog & Ramirez-Ruiz 2002).

Considerable discussion has recently been given to whether the expected r^{-2} density structure for a stellar wind is compatible with the analysis of the afterglow light curves (e.g. Lazzati & Perna 2002; PK02; Price et al. 2002; Chevalier & Li 2000, hereafter CL00). PK02 found that in half of the cases they modelled, a homogeneous ambient medium accommodates the afterglow emission better than the wind-like medium. Although wind-like external medium solutions were reported as being a poor match to the data in the other cases, PK02 include them as possible alternatives for three of the six bursts in our sample: 991208, 991216, and 000418. To adopt the r^{-2} solutions for these three bursts would place their RSs in the radiative (fast cooling) regime. At best, a wind medium radiative RS can attain an optical peak flux which is comparable in magnitude to the homogeneous medium adiabatic case. For typical parameters, however, the optical flux is six times *fainter* in a wind environment than the constant density medium case (CL00). Specifically, the peak flux is given by

$$F_{\nu,\max} = 46(1+X)\left(\frac{1+z}{2}\right)^{1/2}\left(\frac{2-\sqrt{2}}{1+z-\sqrt{1+z}}\right)^{2} \times \left(\frac{\epsilon_B}{0.1}\right)^{-1/4} \frac{E_{52}^{5/4}}{A^{1/2}\Gamma_{0,3}\Delta_{10}^{3/4}}\ \mathrm{mJy} \quad (13)$$

where X is the fractional abundance of hydrogen ($\sim$0 for Wolf–Rayet winds) and A is a constant which describes the density profile of the wind (CL00). This peak corresponds to an optical flash of magnitude $m_V \approx 12$ as compared with an r^{-2} estimated peak of $m_V \approx 9$. Furthermore, the RS emission dies off more rapidly when surrounded by a wind external medium. The ability to detect a RS contribution within early radio observations is then generally reduced for an r^{-2} burst. Therefore, after modelling the early afterglows of 991216 and 991208, which are better described with the addition of a RS contribution, we argue that the homogeneous medium solution is preferred. As a consistency check, we can instead assume the lower limits in the value of Γ_0 given by PK02 and fit for the density of the external medium. By doing so, we find density values that are consistent with those from the FS model, which implies that there is no direct evidence for large-scale clumps within the density profile.

If the progenitors are massive stars then there is an analogy to the explosions of core collapse supernovae, for which there is abundant evidence that they interact with the winds from the progenitor stars. In most supernova cases, the radial range that is observed is only out to a few 10^{17} cm, such that the mass-loss characteristics have not changed significantly during the time that mass is supplied to the wind (CL00). The density in the wind depends on the type of progenitor. Red supergiant stars, which are thought to be the progenitors of Type II supernovae, have slow dense winds. Wolf–Rayet stars, which are believed to be the progenitors of Type Ib/c supernovae and possibly of GRBs (e.g. MacFadyen & Woosley 1999), have faster lower density winds. Deceleration due to this wind starts in earnest when about half the initial energy is transferred to the shocked matter, i.e. when it has swept up Γ_0^{-1} times its own rest mass. The typical mass where this occurs is $M_{\rm ej} = E/(\Gamma_0^2 c^2) \sim 5 \times 10^{-6} E_{53}\Gamma_{0,2}^{-2}\ \mathrm{M}_\odot$ (Mészáros & Rees 1993).

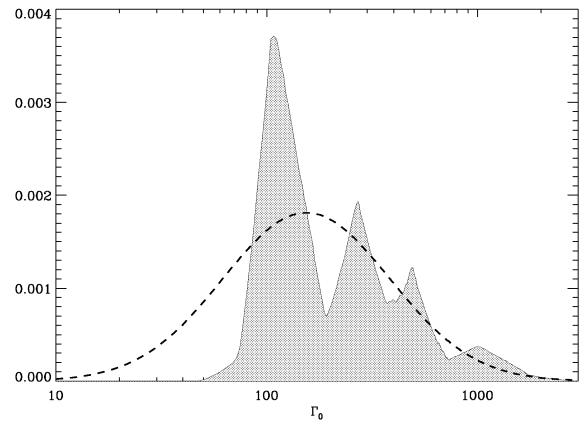

Figure 10. Distribution of GRB Lorentz factors. This distribution is essentially a smooth histogram of the data, but one that takes into account the uncertainties in the measurements. The dashed curve is the distribution under the curve (shaded) but smoothed with a Gaussian with a mean value of $\Gamma_0 = 150$.

Table 1. Constraints on Γ_0 and g obtained by fitting a RS + FS model to early radio observations. The reduced χ^2 for the best FS + RS model is given as well as the ratio $\chi^2_{\rm FS+RS}/\chi^2_{\rm FS}$. For $\chi^2_{\rm FS+RS}/\chi^2_{\rm FS} < 1$, the fit is improved by including emission from the RS.

GRB	Thin regime				Thick regime			
	Γ_0	$g(g_{\rm low} - g_{\rm high})$	$\chi^2_{\rm FS+RS}$	$\chi^2_{\rm FS+RS}/\chi^2_{\rm FS}$	Γ_0	$g(g_{\rm low} - g_{\rm high})$	$\chi^2_{\rm FS+RS}$	$\chi^2_{\rm FS+RS}/\chi^2_{\rm FS}$
980519[a]	490	1.5	12.0	1.4	>230	1.5	–	–
990123	850	3.4	0.3	0.01	240	3.3	0.3	0.01
990510	270	1.5	8.5	8.0	>230	1.5	–	–
991208	110	1.9	1.9	0.5	130	3.5	1.5	0.4
991216	680	1.5	4.2	0.6	1200	1.5	4.2	0.6
000418	150	1.5	9.7	1.0	>50	1.5	–	–

[a]Redshift unknown; $z = 1$ was assumed.

Fig. 11 shows the (isotropic equivalent) swept-up mass as a function of radius derived from our Γ_0 estimates. It should be noted, however, that the afterglows sample a region $\leqslant 10^{17}$ cm ($\sim$0.03 pc) in size. Depending upon the wind history of a Wolf–Rayet star during its last few centuries, the density structure in this region could be quite complicated as the star enters advanced burning stages unlike those in any Wolf–Rayet star observed so far (the uncertainty in the evolution of massive stars leaves open the possibility of interaction with denser material at early times; see, for example, Ramirez-Ruiz et al. 2001). Still, there is no obvious way for the ejected mass at 10^{17} cm to be much lower than about 10^{-5} M$_\odot$ (assuming $\dot{M} = 10^{-6}$ M$_\odot$ yr^{-1} and $v_w \sim 10^3$ km s^{-1}; see the dashed line in Fig. 11). The low swept-up mass inferred is thus problematic for the collapsar model. This has led to the suggestion that the fireball expansion may be taking place inside the constant density medium that is expected downstream from the termination shock of the massive star wind (Wijers 2001; see also Scalo & Wheeler 2001). The radius of the wind termination shock at the inner edge of the wind bubble can be found by balancing the wind ram pressure with the post-shock cavity pressure. The termination shock radius, $R_{\rm t}$, is thus given by

$$R_{\rm t} = 0.4 \dot{M}_{-6}^{3/10} v_{w,3}^{1/10} n_{0,3}^{-3/10} t_6^{2/5} \ {\rm pc} \qquad (14)$$

where t_6 is the lifetime of the star in Myr and n_0 is the interstellar gas density. The density in the uniform shocked wind region, $n_{\rm sw}$, at late times is given by

$$n_{\rm sw} \sim 3\dot{M} \frac{t}{4\pi R_{\rm t}^3 m_{\rm p}} = 0.06 \dot{M}_{-6}^{4/5} n_{0,3}^{3/5} v_{w,3}^{6/5} t_6^{-4/5} \ {\rm cm}^{-3}, \qquad (15)$$

which shows that even if the progenitor star is embedded in a dense molecular cloud the observed blast wave can propagate in a low-density, uniform medium (Wijers 2001). The mass within the $1/r^2$ wind, $M_{\rm t}$, is

$$M_{\rm t} \sim 3 \times 10^{-4} \dot{M}_6^{13/10} v_{w,3}^{-9/10} n_{0,3}^{-3/10} t_6^{2/5} \ {\rm M}_\odot. \qquad (16)$$

A comparison with estimates in Fig. 11 shows that, if the wind is especially weak (i.e. $\dot{M} \sim 10^{-6}$ M$_\odot$ yr^{-1}) or the surrounding pressure is high ($n_0 > 10^3$), $R_{\rm t}$ falls within the range of the relativistic expansion. Considering the radial requirements relevant to our sample, we conclude that this applies to most cases (see Table 2). Models and observations of Galactic Wolf–Rayet stars, however, show that the swept-up shell of a red supergiant material at the outer radius is at a distance $\geqslant$3 pc from the star (Garcia-Segura, Langer & Mac Low 1996). This radius is sufficiently large that the interaction with the free $1/r^2$ wind is expected over the typical period of observation of afterglows. The calculations above demonstrate that a blast wave expanding into a wind bubble only works for massive stars with relatively low mass winds ($\leqslant 10^{-6}$ M$_\odot$ yr^{-1}) and/or embedded in dense molecular clouds $n_0 \geqslant 10^3$ cm^{-3}.

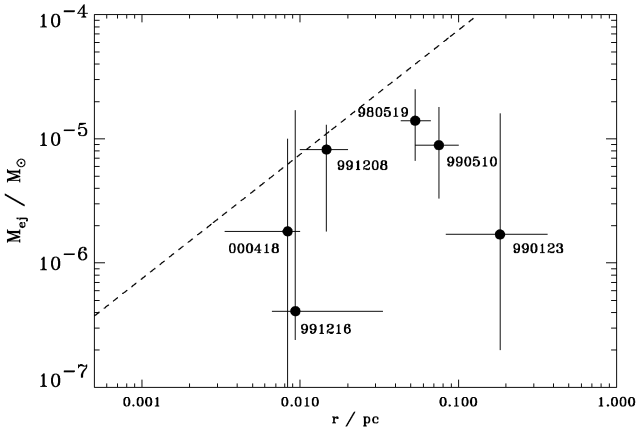

Figure 11. Constraints on the swept-up mass $M_{\rm ej}$ as a function of radius. The dashed curve is the ejected stellar mass assuming $\dot{M} = 10^{-6}$ M$_\odot$ yr^{-1} and $v \sim 10^3$ km s^{-1}. The errors in $M_{\rm ej}$ and radius take into account the uncertainties in the Γ_0 estimates.

Table 2. Wind-bubble parameter constraints for six bursts. Estimates derived by requiring the expanding observed blast wave to propagate in the low-density, (uniform) shocked wind region. Best-fitting parameters of both $M_{\rm ej}$ and deceleration radius are used (see Fig. 11), which together with the inferred circumburst density give $v_{\rm w}$, $\dot{M}$ and n_0 via equations (14), (15) and (16).

GRB	$v_{\rm w}$ (1000 km s^{-1})	$\dot{M}$ (10^{-6} M$_\odot$ yr^{-1})	n_0 (cm^{-3})
980519	0.58	0.3	100.0
990123	0.50	0.015	3.4
990510	1.4	0.2	55.0
991208	1.0	0.7	$>10^4$
991216	1.8	0.08	$>10^4$
000418	1.4	0.9	$>10^4$

Although the interstellar and wind models are the two main types of environment considered for afterglows, there is a different scenario involving a massive star in which the supernova explosion occurs before the GRB (e.g. Vietri & Stella 1998; Dado, Dar & De Rujula 2002; Konigl & Granot 2002; Guetta & Granot 2003). The supernova would expand into the progenitor wind, creating a complex circumburst region in the inner part of the wind. Konigl & Granot (2002) have recently shown, for the case of a pulsar-wind bubble, that the shocked wind has a roughly uniform density, similar to that found in the normal interstellar medium.

6 DISCUSSION

Accepting the inference that the radio flares arise from the RS, we place constraints on Γ_0 and g, and hence on the density profile of the medium in the immediate vicinity of bursts 980519, 990123, 990510, 991208, 991216 and 000418. Unlike the continuous FS, the hydrodynamic evolution of the reverse-shocked ejecta is more sensitive. As we demonstrated, the temperature of the reverse-shocked fluid is found to be non-relativistic for most of these bursts. The hydrodynamics of the *cold* shocked ejecta is very different from that of the *hot* ejecta, which is described by the solution of BM76. Surprisingly, both cases predict rather similar light curves, with decay laws that vary in relatively narrow ranges. Hence, it is unlikely that the non-detection of radio flares is linked to the relativistic regime of their RS. As argued above, the detection of such flares, or firm upper limits, would play an important role in discriminating between *cold* and *hot* shell evolution.

Moreover, the strong dependence of the peak time of this RS emission on the bulk Lorentz factor Γ_0 provides a means to measure this elusive parameter. Indeed, we find the fit quality of the FS + RS model to be *most* sensitive to the parameter value of $t_{\rm peak}$. Our Γ_0 estimates are found to typically lie between 100 and 10^3, well above the lower limits derived from the requirement that GRBs be optically thin to high-energy photons (see LS01). Constrained loosely by equation (1), the peak time is predicted to have a lower limit comparable to the light width of the shell. Unfortunately, the shell width can only be approximated based on the duration of the prompt gamma-ray emission, and consequently the lower limit on $t_{\rm peak}$ involves a significant degree of uncertainty in Γ_0. For this sample of bursts, the $t_{\rm peak}$ values are constrained to a large distribution between 1 and 100 s. An increase in the detection efficiency for RS flares and flashes will allow $t_{\rm peak}$ to be better constrained. Although large localization errors plague attempts at early ($t < 1$ d) radio observations, we have shown that signatures of the radio flare may still be detectable (on top of the FS emission) at times significantly after 1 d. Therefore, we promote the use of this constraining method in cases where a late-time radio flare component would otherwise go unnoticed. Certainly it is true that earlier radio observations are the key to improved flare detection, but until current observational constraints are lifted, we argue that it is sufficient to use observations at $t > 1$ d and still recover useful RS constraints.

Knowing Γ_0, we have then estimated the (isotropic equivalent) swept-up matter at the radius where the afterglow is produced to be $\leqslant 10^{-5}$ $M_\odot$ (it should be noted that the afterglows sample a region $\sim$0.03 pc in size). Provisional upon the density of the interstellar medium, this may be comparable to the wind termination radius; but, unless the wind is especially weak or the surrounding pressure is extraordinary high, the low-density masses inferred here may be problematic for the collapsar model. It is evident that the environment surrounding a massive star at the time of its death is a very opulent one. The complex density structure we see in SN 1987A could be a hint of what exists in some GRBs progenitors – rich behaviour with multiple possible transitions in the observable part of the afterglow. If we see such transitions, they can be fairly constraining on the properties of the progenitors. So far, the only candidate for having shown a shock transition is the flare-up of 970508 1 d after the trigger. Due to the deficiency of early data, this interpretation is only one of many allowable. The prompt optical and radio emission from future bursts will give the opportunity of investigating such transitions in detail.

In summary, we show the potential of modelling early radio afterglow observations in an attempt to understand the physics of the RS. By placing constraints on the properties of GRB shocks we hope to enable improved observational strategies for future flash and flare detections. We show that, although current RS theory predicts a detectable radio flare component for a wide range of Γ_0 and g parameter values, it appears to be observationally supported for only some GRBs. As the sample of well-observed GRB afterglows increases, this method will become applicable to a larger set of bursts thereby forming a more statistically significant data set. Analysis of a larger set will offer improved diagnostics on both the initial Lorentz factor of the collimated fireball and also the density of the burst's immediate environment.

ACKNOWLEDGMENTS

This work was motivated by conversations with and encouragement from A. Panaitescu and P. Kumar. The authors wish to thank E. Berger, A. Blain and D. Frail for helpful comments and discussion. AMS was supported by the NSF GRFP. ER-R thanks CONACYT, SEP and the ORS for support.

REFERENCES

Akerlof C. W. et al., 1999, Nat, 398, 400
Akerlof C. W. et al., 2000, ApJ, 532, L25
Berger E. et al., 2001, ApJ, 556, 556
Blandford R. D., McKee C. F., 1976, Phys. Fluids, 19, 1130 (BM)
Chevalier R. A., Li Z., 2000, ApJ, 536, 195 (CL00)
Dado S., Dar A., De Rujula A., 2002, A&A, 388, 1079
Djorgovski S. G., Frail D. A., Kulkarni S. R., Bloom J. S., Odewahn S. C., Diercks A., 2001, ApJ, 562, 654
Frail D. et al., 2000, ApJ, 538, L129
Garcia-Segura G., Langer N., Mac Low M. M., 1996, A&A, 316, 133
Guetta D., Granot J., 2003, MNRAS, 340, 115
Kehoe R. et al., 2001, ApJ, 554, L159
Kobayashi S., 2000, ApJ, 545, 807
Kobayashi S., Sari R., 2000, ApJ, 542, 819 (KS00)
Konigl A., Granot J., 2002, ApJ, 574, 134
Kulkarni S. R. et al., 1999, ApJ, 522, L97
Lattimer J. M., Schramm D. N., 1976, ApJ, 210, 549
Lazzati D., Perna R., 2002, MNRAS, 330, 383
Lithwick Y., Sari R., 2001, ApJ, 555, 540 (LS01)
MacFadyen A. I., Woosley S. E., 1999, ApJ, 524, 262
Mészáros P., Rees M. J., 1993, ApJ, 405, 278
Mészáros P., Rees M. J., 1999, MNRAS, 306, L39 (MR99)
Mészáros P., Laguna P., Rees M. J., 1993, ApJ, 415, 181
Narayan R., Paczyński B., Piran T., 1992, ApJ, 395, L83
Paczyński B., 1986, ApJ, 308, L43
Paczyński B., 1998, ApJ, 494, L45
Paczyński B., 2001, preprint (astro-ph/0108522)
Panaitescu A., Kumar P., 2000, ApJ, 543, 66
Panaitescu A., Kumar P., 2001a, ApJ, 554, 667
Panaitescu A., Kumar P., 2001b, ApJ, 560, L49
Panaitescu A., Kumar P., 2002, ApJ, 571, 779 (PK02)
Perna R., Belczynski K., 2002, ApJ, 570, 252
Piran T., 1999, Phys. Rep., 314, 575
Price P. A. et al., 2002, ApJ, 572, L51
Ramirez-Ruiz E., Fenimore E. E., 2000, ApJ, 539, 712
Ramirez-Ruiz E., Dray L., Madau P., Tout C. A., 2001, MNRAS, 327, 829
Rosswog S., Ramirez-Ruiz E., 2002, MNRAS, 336, L7
Sari R., Piran T., 1995, ApJ, 455, L143
Sari R., Piran T., 1999, ApJ, 517, L109 (SP99)
Scalo J., Wheeler J. C., 2001, ApJ, 566, 723

Soderberg A. M., Ramirez-Ruiz E., 2002, MNRAS, 330, L24 (SR02)
Vietri M., Stella L., 1998, ApJ, 507, L45
Wang X. Y., Dai Z. G., Lu T., 2000, MNRAS, 319, 1159
Wijers R. A. M. J., 2001, in Costa E., Frontera F., Horth J., eds, Gamma-ray Bursts in the Afterglow Era. Springer, Berlin, XIX, p. 307
Williams G. G. et al., 2000, in Kippen R. M., Mallozzi R. S., Fishman G. J., eds, Gamma-ray Bursts. AIP, New York, p. 250
Woosley S. E, 1993, ApJ, 405, 273

This paper has been typeset from a TEX/LATEX file prepared by the author.